Mem. S.A.It. Vol. 84, 1137

Memorie della

The largest near-IR photometric monitoring survey of ultracool L & T brown dwarfs

P.Å. Wilson[1], A. Rajan[2], J. Patience[2], and F. Pont[1]

[1] Astrophysics Group, School of Physics, University of Exeter, Stocker Road, Exeter EX4 4QL, UK, e-mail: paw@astro.ex.ac.uk
[2] School of Earth & Space Exploration, Arizona State University, Tempe, AZ USA 85281

Abstract. We present the initial results from a large-scale photometric monitoring campaign of 70 L- and T-type brown dwarfs. The targets span the spectral sequence from L0 to T8, and each brown dwarf was observed in the J_s-band over a time period of $\sim$ 3 hours with the SofI instrument on the 3.5 m New Technology Telescope (NTT) at La Silla Observatory. The photometric precision for the measurements was typically better than 1-2% for the majority of the sample. In this proceeding, we concentrate on the largest amplitude variables, and report that 5 targets within the sample exhibit variability at a level of $\sim 2 - 5\%$ over the several hour observation sequence. Of the 5 variables – 2M1010, 2M2139, 2M0136, 2M1828, 2M2228 – 2 of the light curves are the first published indication of variability in these objects – 2M1010 and 2M1828. The L/T transition has been suggested to be a region with a possibility of a higher degree of variability due to patchy clouds. Our survey find large amplitude variables across the L – T spectral range with no preference for the transition.

Key words. Brown dwarfs – Photometry – Variability

1. Introduction

Due to their low mass, brown dwarfs do not achieve stable nuclear burning in their core (e.g. Hayashi & Takano 1963). As the brown dwarf atmosphere cools through the L-T spectral sequence, brown dwarf colours become progressively redder followed by a rapid shift from the red to the blue across the transition from the L-type to the T-type. This transition is best explained by the evolution of the cooling atmosphere of these brown dwarfs whereby the atmosphere evolves to form molecules that eventually form into condensate clouds (Chabrier et al. 2000; Marley et al. 2002; Burrows et al. 2006). When the condensate clouds become too heavy to stay suspended they sink below the photosphere. The presence (or absence) of different opacity sources within the brown dwarf atmospheres impacts the observed colours. This shift in colour happens across a narrow effective temperature range, which is hard for 1-D atmosphere models to reproduce. Patchy clouds might be the explanation of the rapid change in colour observed over a narrow temperature range. An additional consequence of patchy clouds would be variations in the observed flux due to the rotation of the brown dwarf and the evolution of the

Send offprint requests to: P. A. Wilson

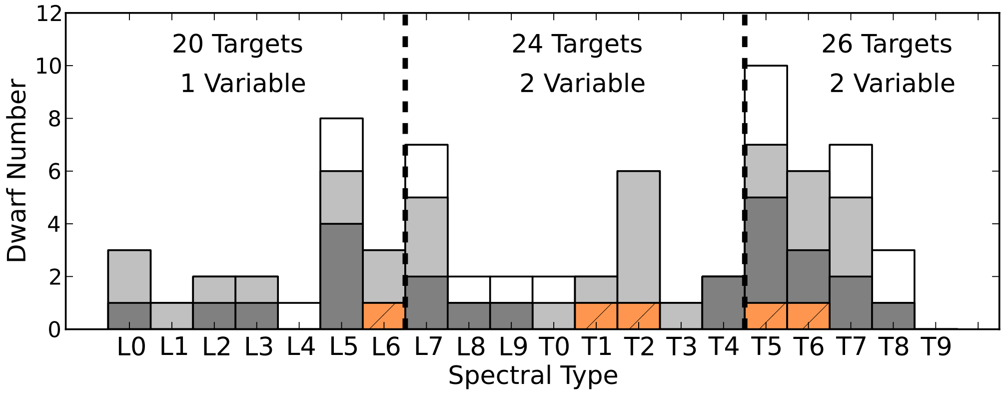

Fig. 1. The spectral-type distribution of all 70 objects in the sample (white) with the transition region defined as L7-T4 (dotted vertical lines). The light grey and dark grey coloured histograms represents photometry better than 2 % and 1 % level respectively. The [orange] hatched histogram represents the variable objects within our sample.

clouds, and our monitoring campaign will investigate this scenario.

2. The Sample

From the brown dwarf archive[1], an initial sample of 78 brown dwarfs were selected to span the full sequence of L- and T- spectral types, with a similar proportion of targets before, within and after the L-T transition region. Among the 78 targets observed, a sample of 70 objects have observations of sufficient duration to search for variability, and a spectral-type distribution of these 70 brown dwarfs are shown in Fig. 1. The spectral types are based on IR spectroscopy for 54 targets and on optical spectroscopy for the remaining 16 targets. The sample consists of 34 targets with known parallaxes (e.g. Dupuy et al. 2012), whilst 8 of the objects are known to be unresolved binaries with four more being binary candidates. All of the binaries in the sample have separations less than the seeing limit, so the photometric measurements in this study record the combined flux from both components. Additional factors that influenced the target selection were the magnitudes and coordinates. The majority of the targets (46 objects) have been observed in programs designed to detect binary companions with radial velocity variations (Blake et al. 2010), spectra showing features of different spectral types (Burgasser et al. 2010), and high angular resolution imaging (e.g. Bouy et al. 2003; Burgasser et al. 2006). Previous observations to search for photometric variability have been reported for approximately half the sample (36 targets). This includes results from optical (Gelino et al. 2002; Koen 2004, 2005, 2013), infrared (Enoch et al. 2003; Clarke et al. 2008; Khandrika et al. 2013) and radio (Berger et al. 2006) observations.

3. Observations

The observations took place during 4th - 11th of October 2011 and 3rd - 9th of April 2012. The entire data set was observed with the SofI (Son of ISAAC) instrument (Moorwood et al. 1998) mounted on the 3.5 m NTT (New Technology Telescope) at ESO La Silla observatory. Three observing blocks, each consisting of two targets, were observed most nights by alternating between the target pair every 15 min over a ∼ 3.2 hour window. This allowed for 6 targets to be observed every night. The observations typically consisted of 25 exposures per 15 min bin with each image typically consisting of a 5s NDIT integration with a DIT length of 5s. Due

[1] www.dwarfarchives.org

Table 1. Largest amplitude variables identified in this study

Object	Spectral Type	DOF	$\chi^2_{\rm red}$	$\tilde{\eta}$	Phot. Quality	Amplitude
2MASS J10101480-0406499	L6 (Opt.)	9	2.9	1.5	0.96%	3.9 ± 1.3%
2MASS J21392676+0220226	T1.5 (IR)	6	15.2	3.1	0.54%	5.3 ± 0.9%
2MASS J01365662+0933473	T2.5 (IR)	7	4.7	1.9	0.42%	2.4 ± 0.7%
2MASS J18283572-4849046	T5.5 (IR)	7	3.3	1.6	0.62%	2.1 ± 0.7%
2MASS J22282889-4310262	T6.5 (IR)	7	3.9	1.4	0.93%	3.4 ± 1.0%

See Wilson et al. (2013) for results on the full sample.

to varying observing conditions such as the presence of thin wispy clouds, and the object being brighter/fainter than initially thought, these times were adjusted. The flux was kept below 10 000 ADUs for the brightest targets in the field to minimise the non-linearity effects. The observing conditions were photometric with only thin cirrus clouds present on the 7$^{\rm th}$ and 8$^{\rm th}$ of April 2012. On the 9$^{\rm th}$ of April, no observations were taken due to a persistent cloud cover. Observations were done in the large field imaging mode, which has a pixel scale of 0.228 arcsec pixel^{-1}. The non-destructive readout mode was not used as it is only offered for spectroscopic modes.

4. Data reduction and photometry

The data reduction was performed using standard IRAF[2] routines which involved flat fielding the images using dome flats, as well as removing large scale sensitivity variations using illumination correction flats. We made use of IRAF scripts provided by the observatory to generate the flats. The sky background was subtracted using the science frames themselves by median combining a pre-determined set of 5 or 10 frames taken before and after the science frame of interest.

The aperture photometry employed the APPHOT package in IRAF. In order to ensure the best possible photometry, a range of apertures were explored. The aperture combination which produced the smallest scatter within each photometric bin, was found to be $\sim 1.2\times$ the median FWHM (full width at half maximum) throughout the sequence and was kept constant for each object. The light curve was produced by dividing the flux from the target by a weighted mean of the normalised reference star fluxes. Candidate reference stars below a signal to noise of S/N$\sim$30 or which showed scatter larger than two times the median absolute deviation were discarded as reference stars. The number of reference stars typically varied between 3 and 12.

We found the dominant systematic effects to be airmass and seeing variations. The light curves were de-trended by first dividing the target light curve by a fit to the normalised flux as a function of the most dominant effect, then by dividing the newly de-trended light curve by a fit to the de-trended normalised flux as a function of the second most dominant effect. We visually inspected each stage of the process to make sure no variability was introduced to the target light curve as a result of FWHM-outliers. The seeing trend was modelled using a linear fit to the FWHM values whilst the airmass trend was modelled by a second order polynomial fit.

The uncertainties were calculated using the largest of either the uncertainties calculated using IRAF or those calculated using the standard deviation of the data points within each bin. These methods provided similar results, but also ensured that we did not underestimate the uncertainties in cases where a smaller number of points within each bin might have made

[2] IRAF is distributed by the National Optical Astronomy Observatories, which are operated by the Association of Universities for Research in Astronomy, Inc., under cooperative agreement with the National Science Foundation.

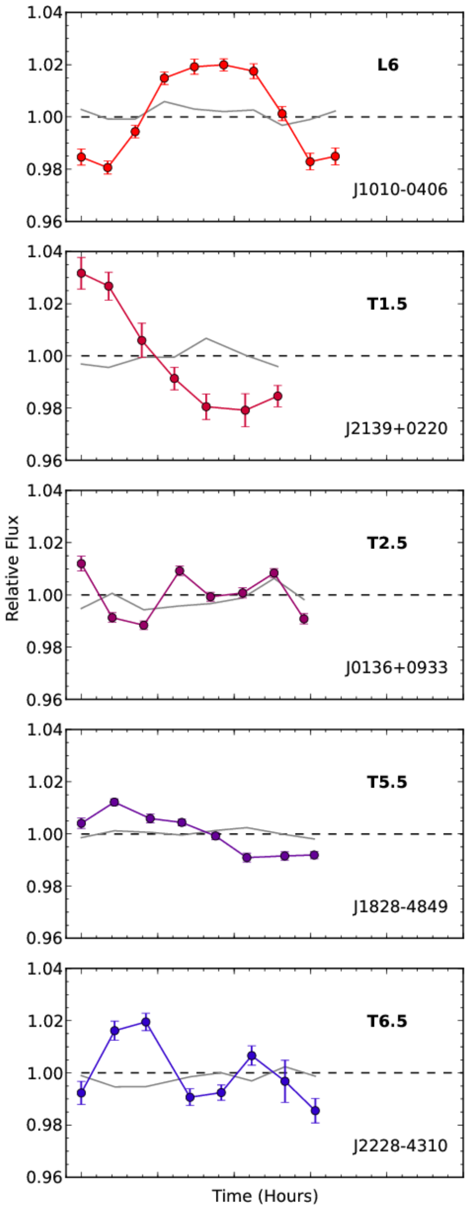

Fig. 2. The light curves of the largest amplitude variable objects found in the in the sample, together with the normalised and median combined reference star light curves (grey line).

the uncertainties based on the standard deviation unreliable.

4.1. Identification of variables

With the uncertainties calculated, the significance of the variations were assessed. The reduced chi squared (χ_r^2) and the reduced robust median statistic ($\tilde{\eta}$, Enoch et al. 2003), where $\tilde{\eta}$ is expressed as:

$$\tilde{\eta} = \frac{1}{d} \sum_{i=1}^{N} \left| \frac{\Delta F_i - \text{median}(\Delta F)}{\sigma_i} \right| \quad (1)$$

with d being the number of free parameters and σ_i, the uncertainty on the binned points, were both calculated relative to a straight line.

The photometric quality of the observations were determined by calculating the median of the standard deviation of each bin within an observing sequence. Objects with a false detection rate $\leq$ 1%, which corresponds to a $\chi_r^2 \geq 2.0 - 2.7$, depending on the degrees of freedom (DOF) and which had $\tilde{\eta} \geq 1$, were considered to be highly variable. Table 1 lists the highest amplitude (min to max) variables passing the criteria set by the reduced chi squared and robust statistic. Some of the variables have higher reported amplitudes, however the previous observations spanned a longer time sequence.

5. Results and discussion

Out of the 70 objects that we have monitored for ~ 3 hours, 5 are variable to a degree that is comparable to other large amplitude variables reported in the literature (see Table 1 and Fig. 2). We confirm the variable nature of three of these brown dwarfs identified and studied in detail by Radigan et al. (2012) for 2M2139, Artigau et al. (2009) for SIMP0136 and Clarke et al. (2008), Buenzli et al. (2012) for 2M2228. The new object 2M1828 has previously been studied and found to be constant in the J-band (Clarke et al. 2008).

Four members of our sample – 2MASS J02284355-6325052, 2MASS J08354256-0819237, 2MASS J09393548-2448279, 2MASS J23312378-4718274 – have been previously reported as variables in Koen (2013) (2M0228, 2M0835) and Clarke et al. (2008)

(2M0939, 2M2331), however, variations are not present in the NTT photometry. In two cases – 2M0228 and 2M0835 – the modulations were measured at a different wavelength (I_c), possibly explaining the different results. The new data may also be an indication of weather patterns that do not persist over the multi-year timespan between the previous and new observations.

We detect variable objects across the L-T spectral range and not just in the L-T transition region (here defined as L7-T4). The variability seen in J1828 and J2228 supports the persistence of sulfide clouds (Morley et al. 2012) amongst mid-T objects.

6. Conclusion

We present the initial results from a variability survey of 70 known early-L to late-T brown dwarfs using the NTT 3.5-m telescope. We detect 5 high amplitude variable objects in the sample, two of which are mid-T dwarfs outside the L-T transition region. We find that variability above the ~ 3%-level at J_s-band wavelengths is rare, even in the L-T transition region. In an upcoming paper (Wilson et al. 2013), we will discuss the frequency of variability including lower amplitude variables. We have extended the variability campaign into the late-T/Y spectral types in a pilot study (Rajan et al. 2013).

Acknowledgements. We are grateful to the organisers for letting us present our work, and for the attendees for their questions and feedback. PAW acknowledges support from STFC.

References

Artigau, É., et al., 2009, ApJ, 701, 1534
Berger, E., et al. 2006, ApJ, 648, 629
Blake, C. H., et al. 2010, ApJ, 723, 684
Bouy, H., et al. 2003, ApJ, 126, 1526
Buenzli, E., et al. 2012, ApJ, 760, 31
Burgasser, A. J., et al. 2006, ApJS, 166, 585
Burgasser, A. J., et al. 2010, ApJ, 710, 1142
Burrows, A., et al. 2006, ApJ, 640, 1063
Chabrier, G., et al. 2000, ARA&A, 38, 337
Clarke, F. J., et al. 2008, MNRAS, 386, 2009
Dupuy, T. J., et al. 2012, ApJS, 201, 19
Enoch, M. L., et al. 2003, AJ, 126, 1006
Gelino, C. R., et al. 2002, ApJ, 577, 433
Hayashi, C., & Takano, T. 1963, Progress of Theor. Phys., 30, 460
Khandrika, H., et al. 2013, AJ, 145, 71
Koen, C., 2004, MNRAS, 354, 378
Koen, C., 2005, MNRAS, 360, 1132
Koen, C., 2013, MNRAS, 428, 2824
Marley, M. S., et al. 2002, ApJ, 568, 335
Moorwood, A., et al. 1998, The Messenger, 91, 9
Morley, C. V., et al. 2012, ApJ, 756, 172
Radigan, J., et al. 2012, ApJ, 750, 105
Rajan, A., et al. 2013, A&A, submitted
Wilson, P., A., et al. 2013, MNRAS, in prep.